AD-A098 568 NAVAL POSTGRADUATE SCHOOL MONTEREY CA F/G 20/4
CONTROL OF AIRFLOW ABOUT A HIGH ENERGY LASER TURRET.(U)
DEC 80 A M MANDIGO
UNCLASSIFIED NPS-80-019 NL

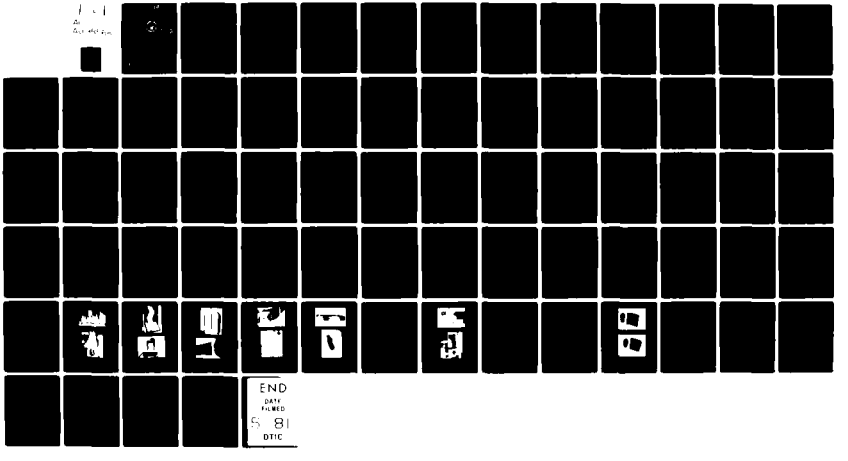

END
DATE FILMED
5 81
DTIC

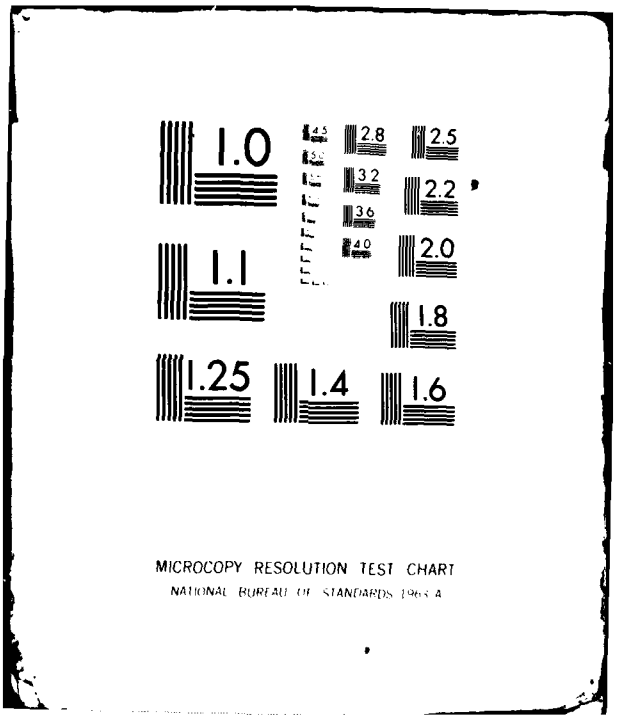
1.0
1.1
1.25
1.4
1.6
1.8
2.0
2.2
2.5
2.8
3.2
3.6
4.0
MICROCOPY RESOLUTION TEST CHART
NATIONAL BUREAU OF STANDARDS 1963 A

NPS67-80-019

LEVEL II

(2)

BS

NAVAL POSTGRADUATE SCHOOL

Monterey, California

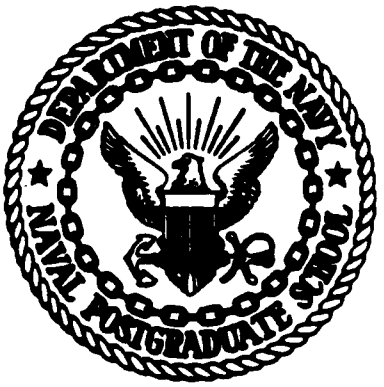

THESIS

CONTROL OF AIRFLOW ABOUT
A HIGH ENERGY LASER TURRET

by

Alan Michael Mandigo

December 1980

Thesis Advisor: A. E. Fuhs

Approved for public release; distribution unlimited

Prepared for: Captain Richard deJonckheere
Air Force Weapons Laboratory
Kirtland Air Force Base
New Mexico 87117

SECURITY CLASSIFICATION OF THIS PAGE (When Data Entered)

REPORT DOCUMENTATION PAGE	READ INSTRUCTIONS BEFORE COMPLETING FORM
1. REPORT NUMBER: NPS67-80-019 (14)	2. GOVT ACCESSION NO.: AD-A098 568
4. TITLE (and Subtitle): CONTROL OF AIRFLOW ABOUT A HIGH ENERGY LASER TURRET.	5. TYPE OF REPORT & PERIOD COVERED: Master's Thesis; December 1980
	6. PERFORMING ORG. REPORT NUMBER
7. AUTHOR(s): Alan Michael Mandigo (10)	8. CONTRACT OR GRANT NUMBER(s): (12)
9. PERFORMING ORGANIZATION NAME AND ADDRESS: Naval Postgraduate School, Monterey, California 93940	10. PROGRAM ELEMENT, PROJECT, TASK AREA & WORK UNIT NUMBERS
11. CONTROLLING OFFICE NAME AND ADDRESS: Naval Postgraduate School, Monterey, California 93940 (11)	12. REPORT DATE: December 1980 13. NUMBER OF PAGES: 71
14. MONITORING AGENCY NAME & ADDRESS(if different from Controlling Office): Naval Postgraduate School, Monterey, California 93940	15. SECURITY CLASS. (of this report): Unclassified 15a. DECLASSIFICATION/DOWNGRADING SCHEDULE

16. DISTRIBUTION STATEMENT (of this Report)

Approved for public release; distribution unlimited

17. DISTRIBUTION STATEMENT (of the abstract entered in Block 20, if different from Report)

18. SUPPLEMENTARY NOTES

19. KEY WORDS (Continue on reverse side if necessary and identify by block number)

Laser, Beam Control, Jitter, Laser Turret, Flow Control, Optical Path Distortion

20. ABSTRACT (Continue on reverse side if necessary and identify by block number)

A high energy laser system inflicts damage on a target by radiating large amounts of thermal energy onto a small area. Airflow about the laser turret, which is located on top of the aircraft fuselage, is unsteady and causes problems in beam control. The problems are jitter, which is vibration of the laser beam, and optical path distortions.

The theory of flow around a cylinder and around a sphere was examined, and several airflow control techniques were screened

DD FORM 1 JAN 73 1473 EDITION OF 1 NOV 65 IS OBSOLETE
S/N 0102-014-6601

SECURITY CLASSIFICATION OF THIS PAGE (When Data Entered)

Block 20 (Cont'd)

in an effort to suppress the unsteadiness of the flow. A fairing and turret base suction apparatus was selected and experimentally tested in a wind tunnel.

During the course of the experiments several parameters were varied as follows: blower flow rate, spacing between turret and fairing nosepiece, and flow rate in five separate ducts. Results of the tests indicate that the fairing and base suction technique eliminates the unsteadiness. Further research and testing are required to develop this technique for actual use on aircraft.

Approved for public release; distribution unlimited

CONTROL OF AIRFLOW ABOUT A HIGH ENERGY LASER TURRET

by

Alan Michael Mandigo
Lieutenant, United States Navy
B.S.M.E., Lowel Technological Institute, 1974

Submitted in partial fulfillment of the requirements for the degree of

MASTER OF SCIENCE IN ENGINEERING SCIENCE

from the

NAVAL POSTGRADUATE SCHOOL
December 1980

Author Alan Michael Mandigo

Approved by: Allen E Fuhs
Thesis Advisor

T.H. Gawain
Second Reader

M. F. Platzer
Chairman, Department of Aeronautics

William M Tolles
Dean of Science and Engineering

ABSTRACT

A high energy laser system inflicts damage on a target by radiating large amounts of thermal energy onto a small area. Airflow about the laser turret, which is located on top of the aircraft fuselage, is unsteady and causes problems in beam control. The problems are jitter, which is vibration of the laser beam, and optical path distortions.

The theory of flow around a cylinder and around a sphere was examined, and several airflow control techniques were screened in an effort to suppress the unsteadiness of the flow. A fairing and turret base suction apparatus was selected and experimentally tested in a wind tunnel.

During the course of the experiments several parameters were varied as follows: blower flow rate, spacing between turret and fairing nosepiece, and flow rate in five separate ducts. Results of the tests indicate that the fairing and base suction technique eliminates the unsteadiness. Further research and testing are required to develop the technique for actual use on aircraft.

COMMENT CONCERNING JOINT RESEARCH EFFORT

This thesis and Flow Control About an Airborne Laser Turret, a thesis by LT James Schonberger [1], were the result of a joint research project. The flow control concept, experimental apparatus with the exception of the fairing nosepiece, and the instrumentation were common to both theses. The experimental results in this thesis are based on the uniform conformal nosepiece. The results in Ref. 1 are for tapered symmetric nosepiece.

A 16 mm movie of the test results using a tapered, symmetric nosepiece is available from:

Distinguished Professor Allen E. Fuhs, Code 67Fu
Department of Aeronautics
Naval Postgraduate School
Monterey, California 93940

TABLE OF CONTENTS

LIST OF FIGURES

LIST OF TABLES

ACKNOWLEDGEMENTS

I would like to acknowledge the support of Captain Richard deJonckheere and the Air Force Weapons Laboratory for providing the funding necessary to conduct this research project.

I would like to express my sincere appreciation to my thesis partner Lieutenant James Schonberger, without whom this thesis might not have been completed.

Most of all, I would like to thank my Thesis Advisor, Dr. Allen E. Fuhs, Distinguished Professor of Aeronautics and Physics and Chemistry. Dr. Fuhs' technical guidance and efforts were factors to the successful completion of the project. Also, I am very grateful to have had the distinct pleasure of having had the professional expertise of Professor T. H. Gawain as a Second Reader.

I would like to thank Supervisory Aerospace Engineering Technicans Robert Besel and Ted Dunton for their technical support in the use of the wind tunnel and the instrumentation.

Additionally, I would like to express my deepest appreciation for the work done by Model Shop Technician Ronald Ramaker. Without his expert precision building of the laser turret and fairing models, this project would not have been completed successfully. Also, I would like to thank Lieutenant Commanders Kenneth Tillotson and Martin Mellor for the time they donated in the preparation of the wind tunnel and model.

I. INTRODUCTION

A. BACKGROUND

A high energy laser weapon system inflicts damage on a target by radiating large amounts of thermal energy onto a small area. The main components of the system are the laser, which gnerates high power radiation, and the beam control subsystem, which aims the laser beam at the target. The airborne portion of the Department of Defense (DOD) High Energy Laser (HEL) Program is being developed at the Air Force Weapons Laboratory, Kirtland Air Force Base, New Mexico. The test bed for the program is the Airborne Laser Laboratory (ALL), which consists of two highly instrumented NKC-135 aircraft.

The laser beam is aimed at the target by the pointer tracker which is part of the beam control subsystem. The pointer tracker is housed on the top of the aircraft inside a laser turret. In flight, the airflow around the turret causes problems in beam control. The beam control problems are jitter and optical path distortions (OPD). Jitter is a vibration of the laser beam that smears the energy focused within a small spot into a larger spot. The time required to damage the target is increased. Jitter is caused, in part, by unsteady pressure loads on the turret and optical components. Optical path distortions, steady and unsteady, are due to shear layers, boundary layers, flow separation and

vortex shedding in the rear of the turret. The flow around the turret also causes increased pressure loading in the separated flow region behind the turret. This increased unsteady pressure is caused by turbulence within the recirculation region. The aiming of a laser through turbulence is a major problem.

Research and experimentation have demonstrated that optical distortion caused by unsteady flow cannot be corrected by adaptive optical systems. Bandwidth requirements exceed current technology.

B. THESIS OBJECTIVE

The primary objective of this thesis is to develop a quiescent airflow around the turret so that jitter and optical path distortions will be minimized. Control of flow separation will ensure that flow will be quiescent well past the current 120 degree point in order that a greater rearward angle can be achieved by the pointer tracker.

II. THEORETICAL FLOW OF INVISCID FLUIDS AND VISCOUS EFFECTS

A. POTENTIAL FLOW ABOUT A CYLINDER

The potential function, Φ, for uniform flow about a cylinder is given by

$$\Phi = Ux + \frac{Ua^2x}{x^2 + y^2} \tag{2-1}$$

in which U is the free-stream flow velocity and a is the radius of the cylinder. Figure II-1 illustrates the coordinate conventions used. Differentiating the potential function with respect to x and y yields the x and y components of velocity in the potential field.

$$u = \frac{\partial \Phi}{\partial x} = U + Ua^2\left(\frac{y^2 - x^2}{(x^2 + y^2)^2}\right)$$

$$v = \frac{\partial \Phi}{\partial y} = \frac{-Ua^2 2xy}{(x^2 + y^2)} \tag{2-2}$$

A change to plane cylindrical coordinates is helpful where $x = r \cos \theta$ and $y = r \sin \theta$. At the surface of the cylinder $r = a$, and the surface velocity components become

$$u = 2U \sin^2\theta$$

$$v = -2U \sin\theta \cos\theta$$

The total surface velocity is then

$$V_s = (u^2 + y^2)^{\frac{1}{2}} = 2U \sin\theta \qquad (2\text{-}3)$$

Utilizing the surface velocity relation, the surface pressure distribution can be calculated. For an incompressible fluid, total pressure, P_0, is

$$P_0 = P + \tfrac{1}{2}\rho V^2 \qquad (2\text{-}4)$$

At infinity, $V = U$; and at the surface, $V = V_s$.
Therefore

$$P_0 = P_\infty + \tfrac{1}{2}\rho U^2 = P_s + \tfrac{1}{2}\rho V_s^2$$

$$P_s - P_\infty = \tfrac{1}{2}\rho (U^2 - V_s^2) \qquad (2\text{-}5)$$

The free-stream dynamic pressure, q , is defined as

$$q = \tfrac{1}{2}\rho U^2 \qquad (2\text{-}6)$$

Substituting equation (2-3) and equation (2-6) into equation (2-5) yields the surface pressure distribution for a cylinder.

$$\frac{P_s - P_\infty}{q} = 1 - 4 \sin^2\theta \qquad (2\text{-}7)$$

The ratio in equation (2-7) is the pressure coefficient.

Figure II-2 is a plot of the pressure distribution of equation (2-7) as well as the pressure distribution about a sphere as developed below.

B. POTENTIAL FLOW ABOUT A SPHERE

The potential function for uniform flow in spherical coordinates about a meridian section of a sphere of radius, a , is

$$\Phi = U(r\cos\theta + \frac{a^3\cos\theta}{2r^2}) \tag{2-8}$$

As before, at the surface, r = a , and the surface velocity components, u and v , become

$$u = \frac{\partial\theta}{\partial r} = U(\cos\theta - \frac{a^3\cos\theta}{a^3})$$

$$v = \frac{1}{r}\frac{\partial\Phi}{\partial\theta} = -\frac{3}{2}U\sin\theta$$

Total surface velocity, V_s , is therefore

$$V_s = \frac{3}{2}U\sin\theta \tag{2-9}$$

Substituting equation (2-9) and equation (2-6) into equation (2-5) yields the surface pressure distribution for a sphere.

$$\frac{P_s - P_\infty}{q} = 1 - \frac{9}{4}\sin^2\theta \tag{2-10}$$

Equation (2-10) is plotted in Figure II-2.

C. VISCOUS EFFECTS AND FLOW SEPARATION

The preceding potential flow theory dealt with flow of a perfect (inviscid) fluid. An inviscid fluid is satisfactory from a mathematical standpoint in that the equations, which offer some insight into the flow pattern, can be solved readily. However, real effects, such as drag and turbulence, are not predicted by this theory. Experimental measurements indicate significant variance from theory, and the degree of variance is strongly dependent on Reynolds number. Reynolds number, Re, is defined as VD/ν, where V is velocity, D is diameter and ν is kinematic viscosity, all in consistent units. Only in the limiting case, as $Re \to \infty$, i.e. $\nu \to 0$, does theory agree with experiment, since $\nu = 0$ implies inviscid flow. Figures II-3 and II-4 depict theoretical static pressure distribution along with actual experimental data for a cylinder and sphere respectively.

Since all real fluids are viscous, the fluid adheres to a wall (or boundary) in the flow; and frictional forces retard the motion of the fluid in a thin layer along the wall. In this thin layer, the velocity of the fluid increases from zero at the wall to the full free-stream velocity in a short distance. The boundary layer was first described by L. Prandtl [2] and accounts for the phenomena of skin friction drag and boundary layer turbulence.

The boundary layer separation at high Reynolds number which may result in turbulence can be explained by considering

the flow about a blunt object, i.e. a circular cylinder (or laser turret). Figure II-5 shows a stylized flow pattern about a cylinder and the corresponding pressure distribution of potential flow. Outside the boundary layer, the flow accelerates from A to B, and the static pressure decreases. Likewise, the flow decelerates from B to C, and the static pressure increases. The decrease in static pressure from A to B is converted into dynamic pressure, which is then converted back into static pressure from B to C, such that the velocities and total pressures at A and C are equal. However, within the boundary layer, considerable friction exists. Furthermore, the external pressure is impressed upon the boundary layer. Because of the frictional forces in the boundary layer, the boundary layer fluid consumes some of the kinetic energy (dynamic pressure) from A to B. As a consequence not enough energy remains to overcome the impressed static pressure gradient from B to C. Eventually, motion of the boundary layer fluid is arrested, and the external static pressure causes the boundary layer fluid to move in the opposite direction. Thus the flow separates; and in a separated flow region at high Reynolds number, the flow becomes turbulent. The separation point, S , is not a fixed point but is dependent upon Reynolds number and body shape. By reducing or eliminating the pressure gradient from B to C, the separation point could be moved (in theory) to the vicinity of point C; and the flow external to the

boundary layer would remain steady. The concept of flow control using a favorable pressure gradient is the essence of the research presented in this thesis.

III. FLOW CONTROL

A. SURVEY OF VARIOUS PROPOSED METHODS

The following proposed methods were presented at a workshop titled Control of Turbulent, Separated Airflow about Aircraft Turrets, sponsored by Captain Richard deJonckheere at the Air Force Weapons Laboratory, Kirtland Air Force Base, New Mexico, on 10 and 11 March 1980 [4].

1. Off-Turret Control

The off-turret control method uses suction through a porous standpipe at the rear of the turret. The suction is used to achieve quiescent airflow around the turret. Figure III-1 is a side view of the off-turret control method. The forward fairing, if installed, would be used to eliminate vorticity at the turret-fuselage junction.

2. Slot Blowing

The slot blowing method attempts to keep the airflow attached to the turret by the use of jets of air. The jets are located at various points on the turret. Figure III-2 is a top view of the geometry for the slot blowing method; the figure also shows the difference between flow with blowing and flow without blowing. The ducting required for the airjets complicates turret design.

3. Base Suction with Trapped Vortices

The base suction with trapped vortices method uses suction through ports that are located on both sides of a fairing located very close to the turret. The suction is used to create, stabilize, and remove vorticity shed into the wake. Figure III-3 is a top and side view of the base suction with trapped vortices method. Note the design of the fairing used.

4. Base Suction

The base suction method uses suction through an array of small holes at the rear of the turret. The suction removes the boundary layer formed on the turret. Figure III-4 is a top view of the base suction method. This is an efficient method, but the method complicates turret design. The complication arises by the fact that the turret turns, but the suction holes must remain downstream in order to establish and retain steady flow.

B. TEST METHOD

A fairing and base suction apparatus was selected and designed for use in this research project. The hardware consists of the turret, fuselage boundary layer bleed, hollow fairing, fairing nosepiece, and a blower. The specifications and designs are covered in Chapter IV.

The fairing and base suction apparatus uses suction through a hollow fairing and fairing nosepiece at the rear

base of the turret. Quiescent airflow around the turret is achieved due to the suction. Figure III-5 is a top and side view of the turret, fairing and fuselage boundary layer bleed.

IV. EXPERIMENTAL APPARATUS

A. WIND TUNNEL

Wind tunnel tests were conducted in the Naval Postgraduate School 5 X 5 foot, low speed tunnel at a maximum velocity of 33 feet per second; the Reynolds number per foot for 33 feet per second is 2.06×10^5. The 5 X 5 foot tunnel was chosen because of availability and physical size. With the one-third scale turret model (D = 16.8 inches), a Reynolds number of about 3×10^5 was achieved. According to Schlicting [3], the value of the Reynolds number for the tests is in the critical range, and turbulent flow will result.

B. BLOWER SPECIFICATIONS

The blower which provides the fairing suction was selected based on flow rate (cubic feet per minute - cfm) and pressure differential (inches of water - inH_2O). Initial calculations, utilizing the proposed fairing inlet area and a velocity equal to twice free-stream velocity, yielded a flow rate of 7200 cfm. Twice the free-stream velocity was chosen from potential flow theory for flow about a cylinder. Potential flow theory also provided the required pressure differential. In order to eliminate the adverse pressure gradient behind the turret model, a minimum pressure differential of three times the free-stream dynamic pressure was desired. Using a free-stream

velocity of 40 feet per second, free-stream dynamic pressure is approximately 0.36 inH_2O. To allow for losses within the ducting and to provide flexibility in possible follow-on experiments with higher velocities and pressure differentials, blower specifications were increased. The final specifications submitted to manufacturers for bids were for a flow rate of not less than 7500 cfm and a pressure differential of not less than 14 inH_2O. Additional specifications included size restrictions and inlet flow control dampers.

The Aerovent Company, Inc., of Piqua, Ohio, was selected as the blower manufacturer as their Backward Inclined Airfoil, model 500, Single Width Single Inlet (B.I.A.-500, SWSI) centrifugal blower met or exceeded all specifications. The Aerovent blower has a capacity of 7700 cfm with a static pressure differential of 14 inH_2O. Figure IV-1 is a photograph of the Aerovent blower and sheet metal which mates the blower to the ducting. The inlet control damper assembly is shown in Figure IV-2 which is a view looking into the mating duct.

C. FAIRING DESIGN

A hollow fairing with four internal ducts was constructed; each duct has a butterfly valve to throttle the flow. The fairing dimensions were such that a maximum turret look-back angle of 150 degrees could be obtained. Pitot-static tubes were installed in each duct for measurement of flow velocities.

Provisions were made for a detachable fairing nosepiece to allow variation of the turret/fairing geometry. Additionally, a plenum allowing for fuselage boundary layer suction at the base of the turret was incorporated into the fairing assembly. Figure IV-3 shows the fairing duct assembly and plenum. Figure IV-4 shows the fairing duct assembly and under turret plenum after installation in the wind tunnel and without the nosepiece attached or the turret installed.

D. FAIRING NOSEPIECE DESIGN

An open inlet nosepiece uniformly conforming to the turret shape at a separation distance of 1.75-inch was constructed. A splitter plate which isolates the flow around each side of the turret was an integral part of the design. Figure IV-5 shows the nosepiece ready for installation. Note the splitter plate. Figure IV-6 shows the 1.75-inch separation between the turret and the mounted nosepiece.

E. TURRET DESIGN

A stylized, one-third scale model of the existing airborne laser turret was constructed based on drawings provided by Captain Richard deJonckheere. The model consists of a hollow 16.8 inch diameter circular cylinder, 9.6 inches in height, topped by a 16.8 inch diameter hemisphere. The turret is mounted on 0.375 inch aluminum plate with a slot for fuselage boundary layer suction.

F. MODEL INSTALLATION

The blower with sheet metal which mates the blower to the ducting was mounted beneath the wind tunnel test section. The test section floor was removed, and the fairing assembly was installed in the test section and mated to the blower assembly. Figures IV-7 and IV-8 are two views of the under-tunnel assembly. Note the flow control damper handles in the duct assembly in Figure IV-8. Figures IV-9 and IV-10 are photographs of the complete model assembly in the tunnel test section.

V. INSTRUMENTATION

A. PRESSURE TAPS

Pressure taps were installed on the turret, in the wind tunnel, and in the duct assembly. As a result of the extensive array of pressure taps, the pressure distribution on the turret surface could be plotted. Knowledge of static pressure permits calculation of local velocity. Table V-1 is a list of the locations of pressure taps. Figure V-1 is a top and side view drawing of the turret giving exact pressure tap locations. By referring to Figure IV-7, the location of the pressure lines attached to the five pitot-static tubes of the under-tunnel duct assembly can be seen. These lines are for static and dynamic pressure.

B. WIND TUNNEL DATA ACQUISITION SYSTEM

The wind tunnel data acquisition system used in this research project consisted of an INTEL 80/10 Computer System, an AN/UGC-59A Teletypewriter Set, a 48 port Scanivalve, and a digital display unit for the Scanivalve. Figure V-2 is a photograph of the computer system, teletypewriter, and digital display unit. Figure V-3 is a photograph of the Scanivalve.

A control program for the Scanivalve was developed so that the pressure at each of the 48 ports could be measured.

Each port of the Scanivalve is attached to its corresponding pressure tap via Tygon plastic tubing.

The measured quantity for each pressure tap was a dimensionless number related to the voltage across a capacitor pressure transducer located in the bottom of the Scanivalve. To convert the measured values to a useful form, the following calibration procedure was used. Using a U-tube, readings were taken and plotted for each centimeter of water pressure from 0-10 centimeters. The plot determined that the readings were linear so that the equation of a straight line could be used for conversion purposes,

$$y = mx + b \qquad (5\text{-}1)$$

where y is pressure in centimeters of water, and x is the dimensionless measured value. From the calibration procedure, numerical values for m and b were obtained. The results were m = 9.2608 and b = 0.0269. The pressure readings were used to calculate the pressure coefficients and the velocities in the wind tunnel and ducting. Appendix A is an outline of the procedure used to calculate velocities, and Appendix B is an outline of the procedure used to find the pressure coefficients.

C. TUFTS

In order to evaluate qualitatively the steadiness of the airflow, horizontal rows of tufts were taped to the turret. The tufts were made of a light yarn so that small

airflow velocities caused displacement of the tufts. If the flow around the turret was turbulent, the tufts would fly in all directions. When the flow was quiescent, the tufts would lie flat in the direction of flow.

VI. EXPERIMENTAL RESULTS

A. TESTING PROCEDURE

1. Turret-Fairing Nosepiece Separation Distance of 1.75-inches with No Suction

The turret, fairing and the fairing nosepiece were set up in the wind tunnel with a 1.75-inch separation distance between the turret and fairing nosepiece. Test runs were made with no blower suction to obtain the pressure distribution over the turret surface. The pressure distributions were compared with pressure distributions reported in Schlicting [3]. The pressure distributions reported by Schlicting [3] at the calculated Reynolds number of 3×10^5 were in good agreement with the measured pressure distributions; see Section VI-B-1.

2. Turret-Fairing Nosepiece Separation Distance of 1.75-inches with Blower Damper Half Open

Test runs were made with the blower damper open half way to determine the initial effectiveness of the fairing and base suction apparatus which is described in Chapter III-B.

3. Turret-Fairing Nosepiece Separation Distance of 1.75-inches with Variable Suction

Test runs were made with the turret-fairing nosepiece separation distance at 1.75-inches. During the test runs the blower suction, fuselage boundary layer bleed and airflow through the under-tunnel duct assembly were varied.

The purpose of the test runs was to determine an optimum flow configuration that would use minimum blower suction to achieve quiescent airflow around the turret.

4. Turret-Fairing Nosepiece Separation Distance of 2.625-inches with Variable Suction

Test runs were made with the turret moved forward to increase the turret-fairing nosepiece separation distance. Due to the location of the fuselage boundary layer plenum, the maximum separation distance that could be achieved was 2.625 inches. Test runs were made at the 2.625-inch separation distance to determine the optimum flow configuration to achieve quiescent airflow around the turret.

B. TESTING RESULTS

1. Turret-Fairing Nosepiece Separation Distance of 1.75-inches with No Suction

Pressure readings were recorded by the wind tunnel data acquisition system, and pressure coefficients were calculated using the procedure outlined in Appendix B. Figure VI-1 is a plot of the pressure distribution at the expected Reynolds number of 3×10^5 as compared to similar data from Schlicting [3]. The data plotted from the test run are between the observed data at Reynolds numbers of 6.7×10^5 and 1.86×10^5. A comparison indicates that 3×10^5 is a good estimate for the Reynolds number.

2. Turret-Fairing Nosepiece Separation Distance of 1.75-inches with Blower Damper Half Open

Pressure coefficients that resulted from the test run with the blower damper half open and all ducts open are plotted in Figure VI-2. The theoretical pressure distribution plotted in Figure VI-2 shows the expected adverse pressure gradient at the rear of the turret. The pressure distribution from the test run conducted at a separation of 1.75-inches shows a decrease in the pressure gradient at the rear of the turret. The decreased pressure gradient indicates that the suction does work.

3. Turret-Fairing Nosepiece Separation Distance of 1.75-inches with Variable Suction

Test runs were made using many flow configurations until the optimum configuration was found. Quiescent airflow around the turret was achieved when the tufts were steady and aligned with the local flow. Figure VI-3 is a photograph of the turret and fairing nosepiece with wind tunnel on but without blower suction. Note the disarray of the tufts. Figure VI-4 is a photograph of the turret and fairing nosepiece with suction; Figure VI-4 was taken after the optimum flow configuration was achieved. Note that all of the tufts lie flat in the direction of flow, left to right. The optimum flow condition was achieved with the blower open to provide 18 percent of maximum flow, fuselage boundary layer bleed open 25 percent and the inlet ducts 1 to 4 open 100 percent, 100 percent, 50 percent, and 90 percent respectively.

Pressure coefficients were evaluated for the 1.75-inch turret-fairing nosepiece separation distance and are plotted in Figure VI-2. The 1.75-inch separation distance with optimum flow control configuration shows a flattened pressure distribution at the rear of the turret. The flattened pressure distribution means that boundary layer on the turret flows into a neutral pressure gradient.

The accuracy of pitot-static measurements of velocities in the ducting system taken during the testing were questionable due to a high degree of variance between successive measurements. Therefore, instead of using the procedure outlined in Appendix A for finding the velocities, an alternate method of estimating the inlet velocities was made. The method was based on volume flow rate, area ratio and velocity ratio. Appendix C is an outline of the procedure used to estimate the velocities. The velocities at the inlet of the four ducts and the fuselage boundary layer bleed in feet per second were estimated to be 28.65, 24.28, 20.61, 19.36 and 19.36 respectively.

The turret and fairing apparatus used in the experiment were one-third scale of the actual equipment. To determine if this fairing nosepiece design were feasible, dimensions must be scaled to full size. Appendix D is an outline of the procedure used in the scaling. In addition, Appendix D estimates the performance of a fairing and base suction system for full scale at $M_\infty = 0.5$. Volume flow rate and

pressure difference across the blower were claculated and are tabulated in Table VI-1. The results show that the volume flow rates and pressure differences are obtainable with present technology.

The minimum fairing inlet suction area A_s would occur with choked flow, i.e. with $M_s = M^* = 1.0$. The value of the minimum allowable fairing inlet suction area is calculated by assuming $A_s = A^*$ and $A_\infty = FA_t$. Liepmann and Roshko [5] list the area ratio for choked flow at $M_\infty = 0.5$ as $A^*/A_\infty = 0.7464$. With the area factor, F, from experimental results, $A_\infty = FA_t = (0.398)(17.1) = 6.81\ ft^2$, and $A_s = 0.7464A_\infty = 5.08\ ft^2$ for the required suction area. However, the fairing inlet area of the test model, if scaled to full size, would equal $8.76\ ft^2$. To summarize, model $A_s = 0.974\ ft^2$, full scale $A_s = 8.76\ ft^2$, model $A_t = 1.9\ ft^2$, full scale $A_t = 17.1\ ft^2$, full scale $A^* = 5.08\ ft^2$, model $A_\infty = 0.756\ ft^2$ and full scale $A_\infty = 6.81\ ft^2$. Therefore, the above computation indicates that the fairing inlet used in this experiment was $3.6833\ ft^2$ larger than required for the actual aircraft configuration. The inlet to the fairing should not choke.

The turret-fairing nosepiece separation distance of 1.75-inches provides steady airflow around the turret at a low blower suction volume flow rate (18 percent of blower maximum flow capacity). The disadvantage of a small separation distance is the restriction on rearward look angle for the laser beam. The look angle for the 1.75-inch

turret-fairing nosepiece separation distance is 125°; the beam diameter is assumed to be one-half of turret diameter. This is a larger look angle than the current capability of 120° but is little geometrical improvement.

4. Turret-Fairing Nosepiece Separation Distance of 2.625-inches with Variable Suction

Test runs were made using many flow configurations until the optimum configuration was found and quiescent airflow around the turret was achieved. The optimum flow condition was achieved with the blower open to provide 28 percent of maximum flow, fuselage boundary layer bleed open 25 percent and the inlet ducts 1 to 4 open 100 percent, 100 percent, 50 percent, and 90 percent respectively. For identification of duct numbers, see Appendix C, first paragraph.

Pressure coefficients were evaluated for the 2.625-inch turret-fairing nosepiece separation distance and are plotted in Figure VI-2. The 2.625-inch separation distance with optimum flow control configuration shows a flattened pressure distribution at the rear of the turret. The flattened pressure distribution indicates that the increased turret-fairing separation distance also causes the boundary layer on the turret to flow into a neutral pressure gradient.

Using the procedure outlined in Appendix C, velocities at the inlet of the four ducts and the fuselage boundary layer bleed in feet per second were estimated to be 37.34, 35.39, 30.61,

25.58, and 25.23 respectively. Volume flow rate and pressure difference across the blower were calculated using the procedure outlined in Appendix D, and the results are tabulated in Table VI-1. The calculations show that the volume flow rates and pressure differences are greater than the values attained for the 1.75-inch separation distance but are obtainable.

Considering compressibility effects, choked flow at the inlet and using the area factor, F = 0.619, the minimum required fairing inlet suction area A_s was 7.9 ft^2. The test model, if scaled to full size, would be 8.76 ft^2 as stated in section 3. To summarize, model A_s = 0.974 ft^2, full scale A_s = 8.76 ft^2, model A_t = 1.9 ft^2, full scale A_t = 17.1 ft^2, full scale A* = 7.9 ft^2, model A_∞ = 1.18 ft^2 and full scale A_∞ = 10.58 ft^2. Therefore, the computation indicates that even with the turret-fairing separation distance increased from 1.75 to 2.625-inches, the fairing inlet used is 0.8633 ft^2 larger than required for the actual aircraft configuration. Hence, choked flow is avoided.

The 2.625-inch turret-fairing nosepiece separation distance increases the rearward look angle to 130° which is an advantage. The disadvantage is the fact that blower suction was increased by 55 percent.

VII. CONCLUSIONS AND RECOMMENDATIONS

A. CONCLUSIONS

The concept of a fairing and base suction as a method to control the airflow about a laser turret has been proven to be very effective at low free-stream velocity and critical Reynolds number. Scaling of the results indicated that the concept should be successful for transonic velocity, but actual tests are required to prove the concept.

B. RECOMMENDATIONS

A model should be built and tested in a transonic wind tunnel in order to determine how well fairing and base suction controls airflow.

The fairing nosepiece geometry should be altered and tested so that a larger rearward look angle can be accomplished.

APPENDIX A

CALCULATION OF VELOCITIES

The calculation procedure determined that $y = 9.2608x + 0.0269$ where y is the presssure in centimeters of water, and x is the dimensionless measured value. The pressure was converted from centimeters of water to pressure in inches of water as follows

$$(y \text{ centimeters of water})(0.3937 \frac{\text{inches}}{\text{centimeters}}) = y \text{ inches of water} \quad \text{(A-1)}$$

By the use of a conversion equation, the pressure in inches of water was converted to velocity in feet per second

$$(y \text{ inches of water})^{\frac{1}{2}}(4006) = z \frac{\text{feet}}{\text{minute}} \quad \text{(A-2)}$$

$$\frac{(z \frac{\text{feet}}{\text{minute}})}{(60 \frac{\text{seconds}}{\text{minute}})} = z \frac{\text{feet}}{\text{second}} \quad . \quad \text{(A-3)}$$

APPENDIX B

EVALUATION OF THE PRESSURE COEFFICIENT

The pressure coefficient as given in equation (2-7) is defined as

$$\text{pressure coefficient} = \frac{P_s - P_\infty}{q} \quad , \qquad \text{(B-1)}$$

where P_s is the static pressure at point of interest, P_∞ is static pressure in the wind tunnel, and $q = P_d - P_\infty$ is free-stream dynamic pressure, which is the difference between wind tunnel total pressure (P_d) and wind tunnel static pressure. Substituting for q yields

$$\text{pressure coefficient} = \frac{P_s - P_\infty}{P_d - P_\infty} \quad . \qquad \text{(B-2)}$$

Since the calibration equation used in converting the dimensionless measured values for each term in the equation is the same, the calibration factor can be factored and cancelled. Equation (B-2) is used to obtain the pressure coefficient by using only the dimensionless measured values.

APPENDIX C

ESTIMATION OF VELOCITIES

Estimation of the velocities in the 4 inlet ducts, numbered 1 to 4 from top to bottom, and the fuselage boundary layer bleed, duct number 5, was based on volume flow rate, Q, area ratio, and velocity ratio. (Subscript d refers to the blower duct.)

$$Q = V_d A_d = V_1 A_1 + V_2 A_2 + V_3 A_3 + V_4 A_4 + V_5 A_5 \qquad \text{(C-1)}$$

Rearranging equation (C-1) yields:

$$1 = \frac{V_1 A_1}{V_d A_d} + \frac{V_2 A_2}{V_d A_d} + \frac{V_3 A_3}{V_d A_d} + \frac{V_4 A_4}{V_d A_d} + \frac{V_5 A_5}{V_d A_d} \qquad \text{(C-2)}$$

The pressure relation

$$\tfrac{1}{2}\rho V_i^2 = P_0 - P_i \qquad \text{(C-3)}$$

is solved for V_i, and knowing that

$$P_0 = P + q = \text{constant} \qquad \text{(C-4)}$$

the velocity ratio, V_i/V_j, is formed,

$$\frac{V_i}{V_j} = \left[\frac{1 + \frac{P - P_i}{q}}{1 + \frac{P - P_j}{q}}\right]^{\frac{1}{2}} = \left[\frac{1 - \frac{\Delta P_i}{q}}{1 - \frac{\Delta P_j}{q}}\right]^{\frac{1}{2}} \qquad \text{(C-5)}$$

Solving equation (C-1) for V_1/V_d results in an expression of velocity ratios which can be calculated from equation (C-5) and known area ratios.

$$\frac{V_1}{V_d} = \left[\frac{A_1}{A_d} + \frac{V_2A_2}{V_1A_d} + \frac{V_3A_3}{V_1A_d} + \frac{V_4A_4}{V_1A_d} + \frac{V_5A_5}{V_1A_d}\right]^{-1} \qquad \text{(C-6)}$$

The areas in square feet for the inlet ducts, 1 to 4, the fuselage boundary layer bleed and the blower duct were 0.285, 0.186, 0.471, 0.0317, 0.410, and 2.64 respectively. In order to account for the use of the variable dampers in the ducts, a proportionality factor, f, which relates the percentage a duct is open, is introduced into equation (C-6).

$$\frac{V_1}{V_d} = \left[f_1\frac{A_1}{A_d} + f_2\frac{V_2A_2}{V_1A_d} + f_3\frac{V_3A_3}{V_1A_d} + f_4\frac{V_4A_4}{V_1A_d} + f_5\frac{V_5A_5}{V_1A_d}\right]^{-1} \qquad \text{(C-7)}$$

The pressure coefficients, $\Delta P_i/q = (P_s - P)/q$, can be estimated using interpolated values for the midpoint of each inlet based on measured pressure coefficients at the 180° point on the turret. The estimated pressure coefficient values were; $\Delta P_1/q = -8.6$, $\Delta P_2/q = -5.9$, $\Delta P_3/q = -4.0$, $\Delta P_4/q = -3.4$, and $\Delta P_5/q = -3.4$ for the turret at 1.75-inch separation distance and $\Delta P_1/q = -6.9$, $\Delta P_2/q = -6.1$, $\Delta P_3/q = -4.3$, $\Delta P_4/q = -2.7$ and $\Delta P_5/q = -.26$ for the 2.625-inch. The proportionality factors, f, were the same for both separation distances and were $f_1 = 1.0$, $f_2 = 1.0$, $f_3 = 0.5$, $f_4 = 0.9$, $f_5 = 0.25$.

The blower velocity, V_d, was estimated using data provided by the blower manufacturers for Q at 100 percent as being equal to 7700 cubic feet per minute. Hence

$$V_d = \frac{Q}{A_d} \qquad \text{(C-8)}$$

The Q is based on the percentage of the maximum flow used to attain the optimum configuration for each run.

Knowing the values for the areas, pressure coefficients, proportionality factors and velocity ratios, the velocity at the inlets of the 4 ducts and the fuselage boundary layer bleed can be found.

APPENDIX D

PERFORMANCE OF FAIRING AND BASE SUCTION FOR FULL SCALE AT $M_\infty = 0.5$

The cross-sectional area of the upstream streamtube, A_∞, in the wind tunnel corresponding to Q is

$$A_\infty = \frac{Q}{V_\infty} \tag{D-1}$$

where Q is known for each separation distance and V_∞, the average wind tunnel velocity, is 30.55 feet per second. The value of A_∞ is compared with the presented area of the turret, A_t. A_t is 1.9 ft^2 for the one-third scale model. An area factor, F, is defined as

$$F = \frac{A_\infty}{A_t} \tag{D-2}$$

The area factor is used to scale the test data to the actual aircraft configuration at a flight velocity, $M_\infty = 0.5$.

The required flow rate, Q_r, determined for incompressible flow is

$$Q_r = (Fa_\infty M_\infty A_t)(60 \text{ sec/min}) \quad \text{cfm} \tag{D-3}$$

where A_t now represents the full-scale turret presented area. A_t = 17.1 ft^2 for full scale laser turret.

The required pressure differential, ΔP_r, for the aircraft suction device is estimated based on the turret pressure at the 180° point. The pressure differential factor is

$$n = (\Delta P/q)_{180} = (1 - \Pi_r)\frac{P_{180} - P_\infty}{q_\infty} \qquad \text{(D-4)}$$

where P_{180} is the static pressure at the 180° point on the turret. The symbol Π_r denotes pressure recovery of a subsonic diffuser located between the inlet port of the fairing nose-piece and the entrance to the aircraft suction device; Π_r is the ratio of stagnation pressures at the two stations. A value of 0.7 was assumed for Π_r. Values of pressure coefficient can be obtained from Figure VI-2. Rearranging and expanding equation (D-4) gives

$$\Delta P_r = nq_\infty = n\frac{\gamma}{2}P_\infty M_\infty^2 \qquad \text{(D-5)}$$

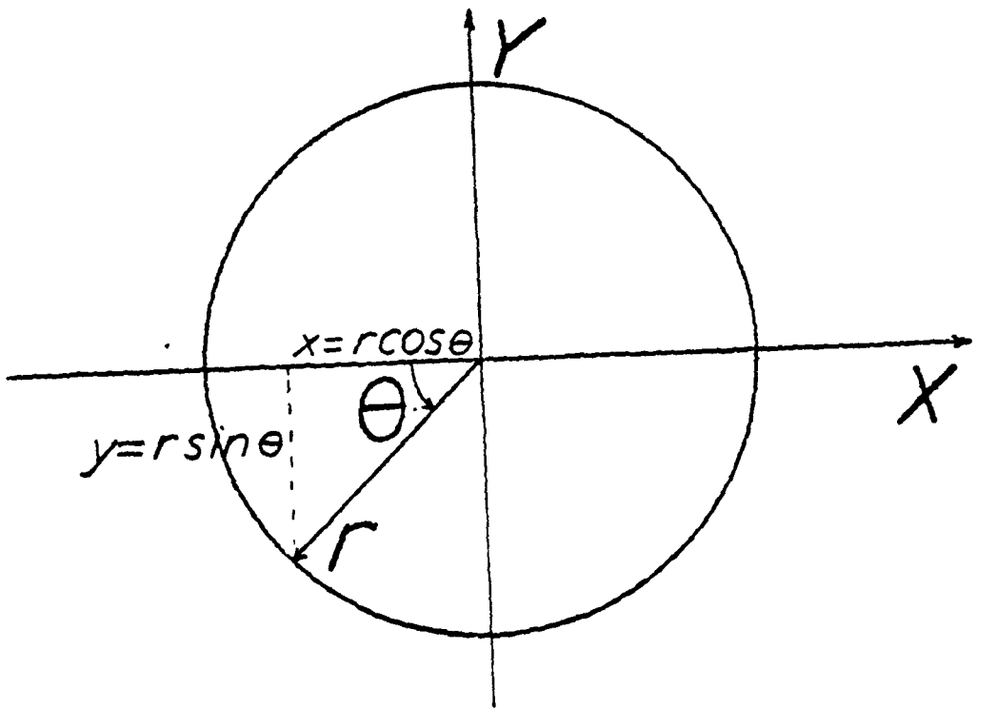

FIGURE II-1. COORDINATE CONVENTIONS USED.

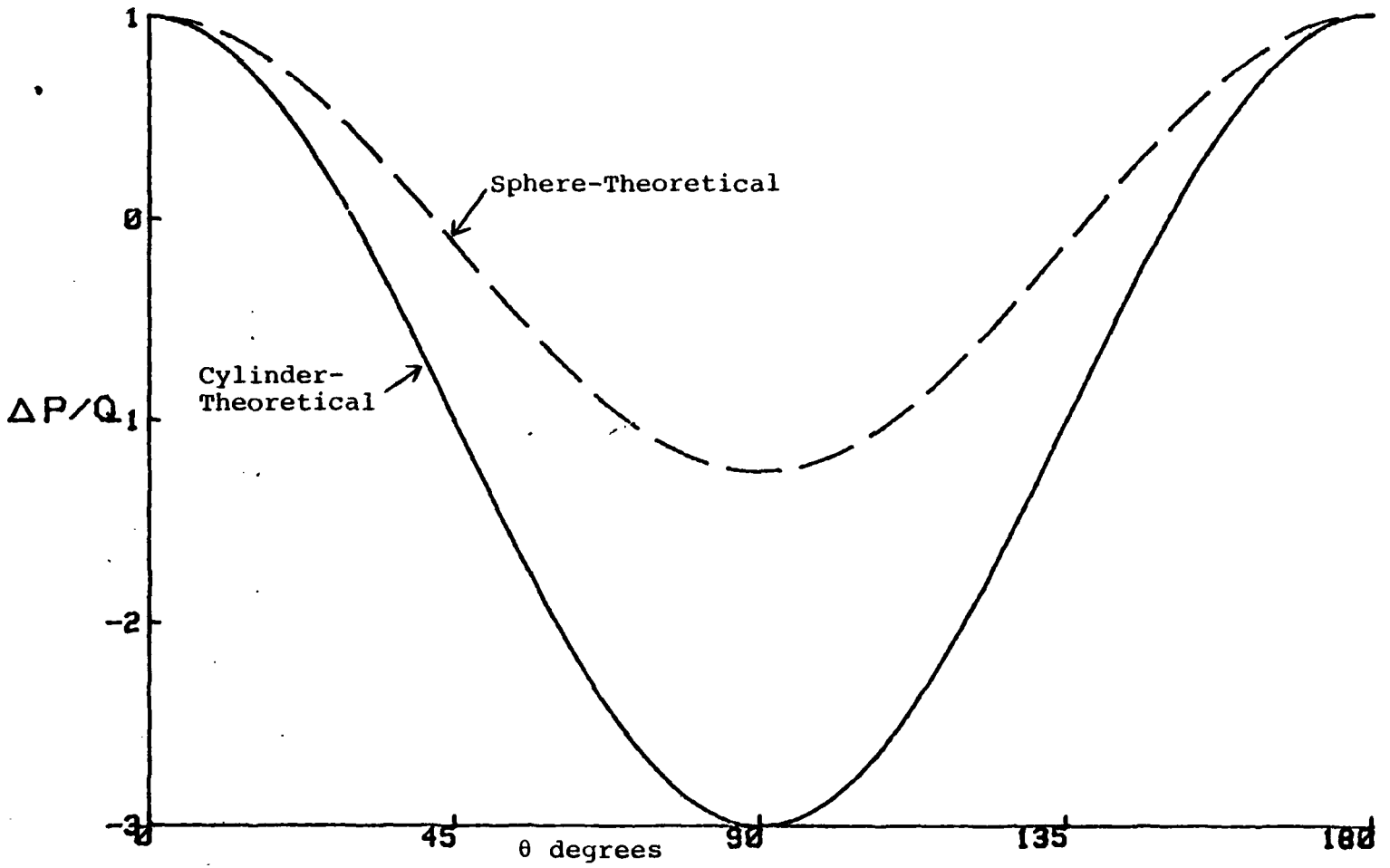

FIGURE II-2. THEORETICAL PRESSURE DISTRIBUTION ABOUT A CYLINDER AND A SPHERE. FROM SCHLICTING [2].

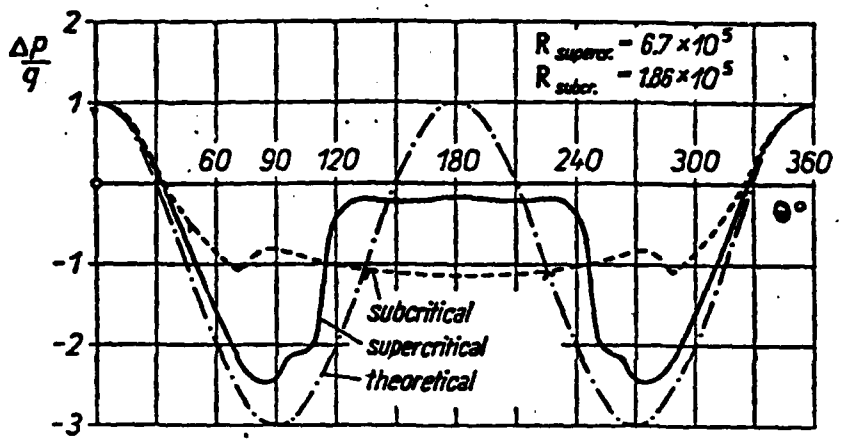

FIGURE II-3. PRESSURE DISTRIBUTION ABOUT A CYLINDER IN SUBCRITICAL AND SUPERCRITICAL RANGE OF REYNOLDS NUMBER. FROM SCHLICTING [2].

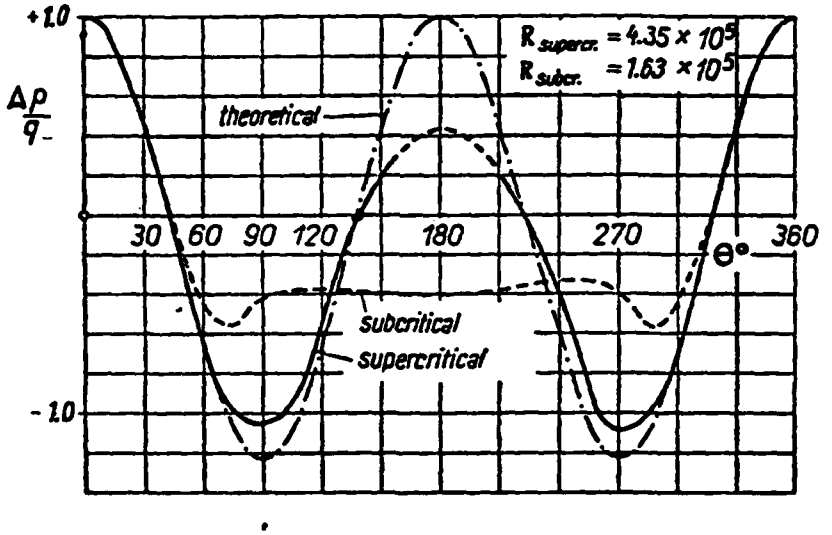

FIGURE II-4. PRESSURE DISTRIBUTION ABOUT A SPHERE IN SUBCRITICAL AND SUPERCRITICAL RANGE OF REYNOLDS NUMBER. FROM SCHLICTING [2].

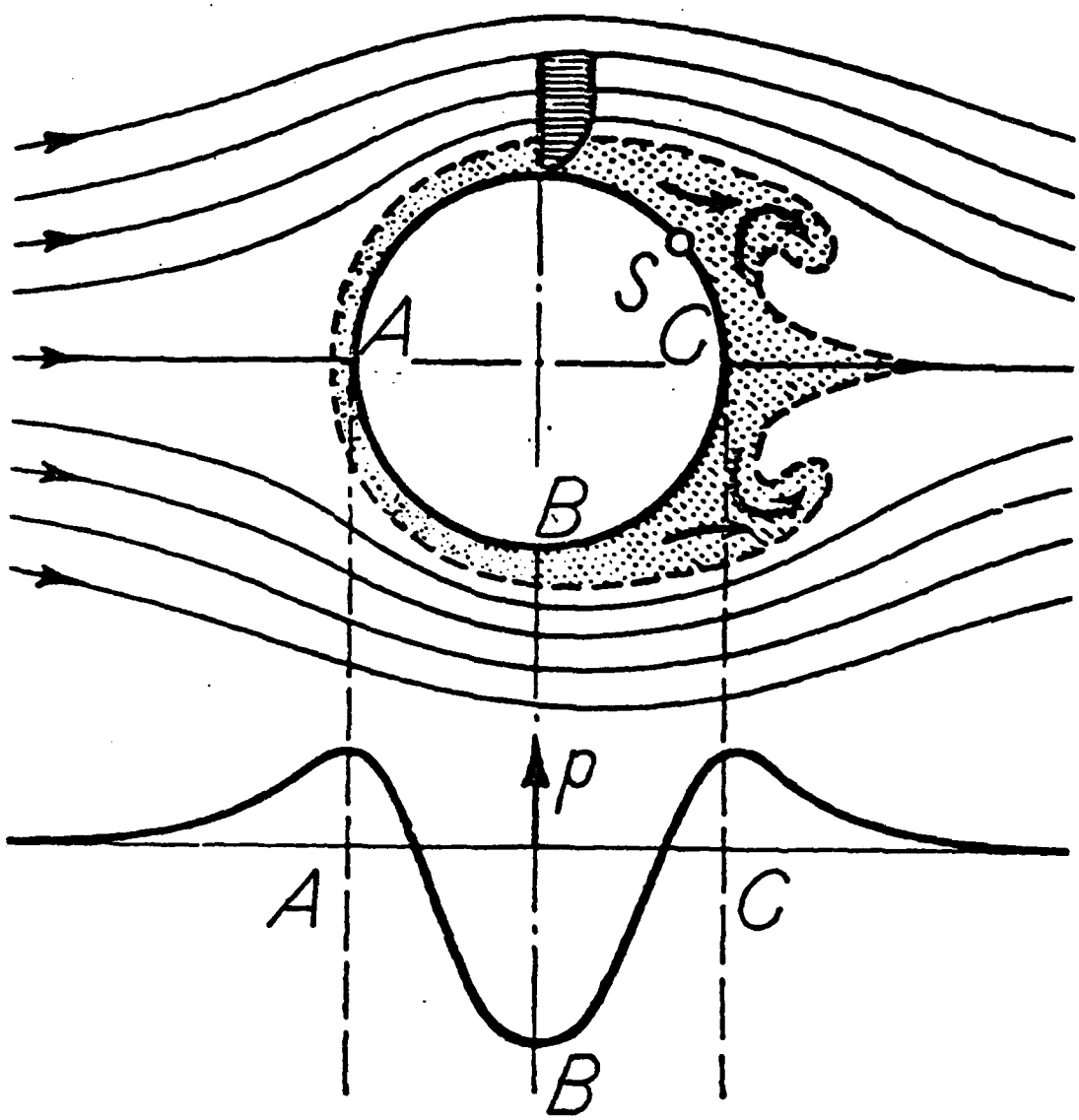

FIGURE II-5. BOUNDARY LAYER SEPARATION AND VORTEX FORMATION ON A CIRCULAR CYLINDER (DIAGRAMMATIC). FROM SCHLICTING [2].

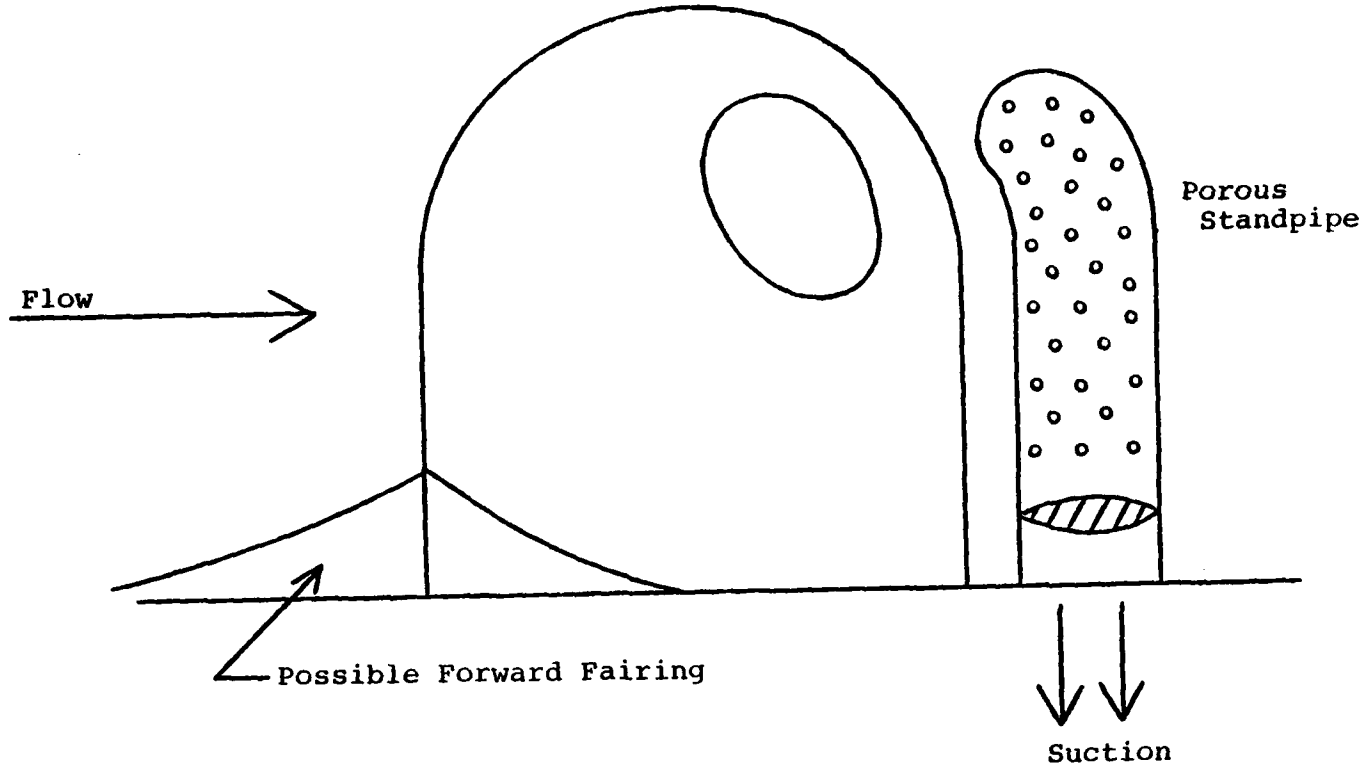

FIGURE III-1. OFF TURRET CONTROL. FROM deJONCKHEERE [3].

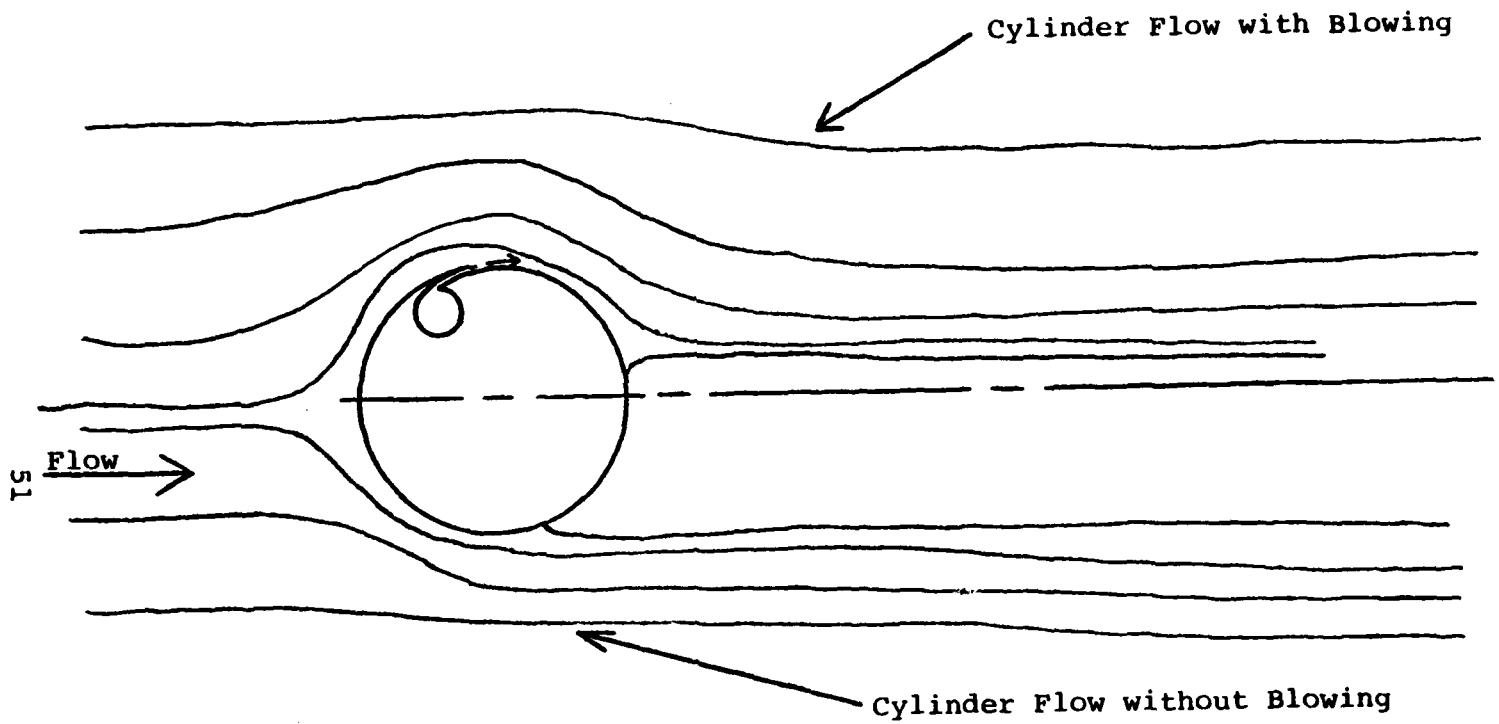

FIGURE III-2. SLOT BLOWING. FROM deJONCKHEERE [3], PRESENTED BY SPECTRON DEVELOPMENT LABORATORIES, INC.

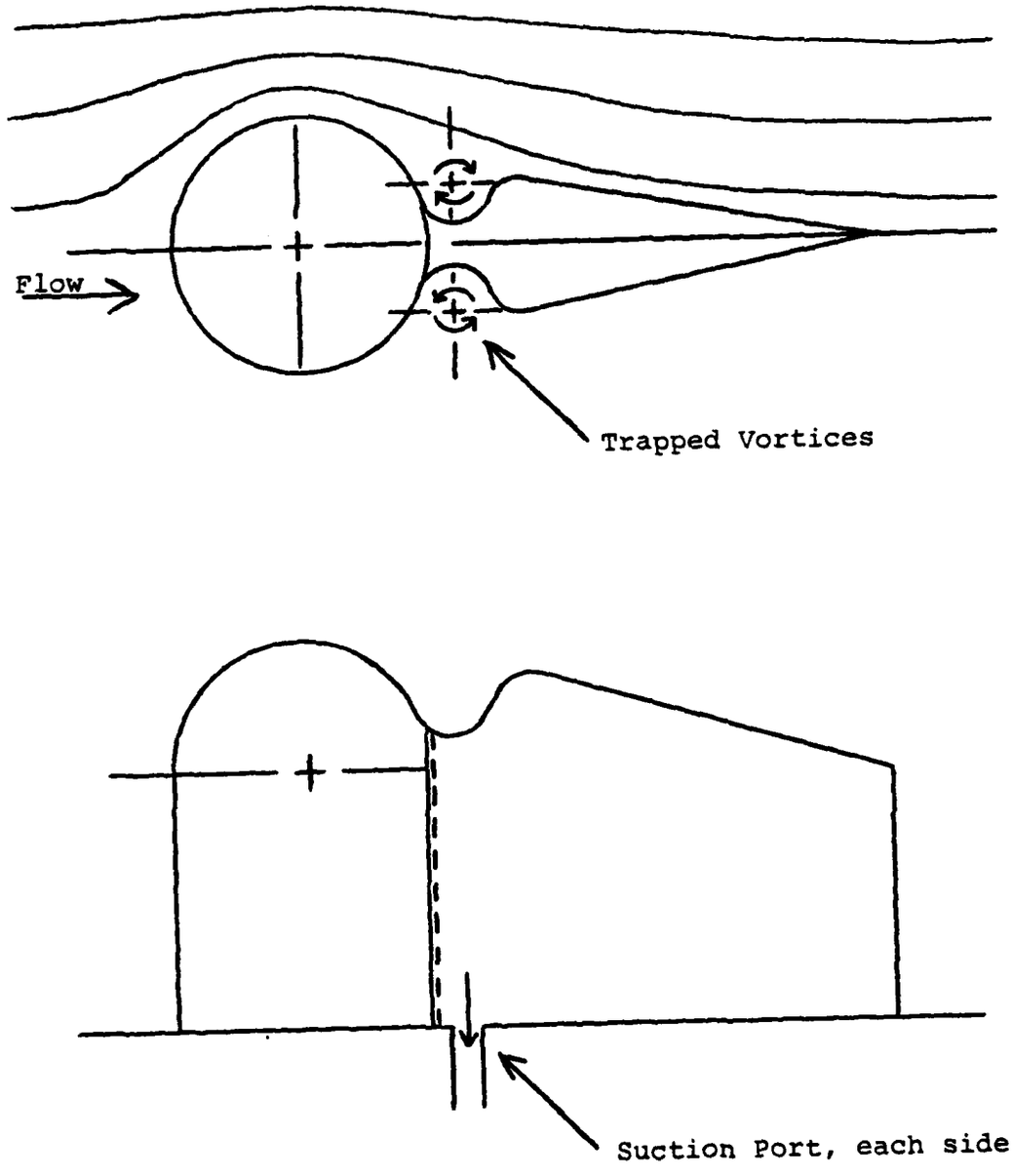

FIGURE III-3. BASE SUCTION WITH TRAPPED VORTICES. FROM deJONCKHEERE [3], PRESENTED BY SPECTRON DEVELOPMENT LABORATORIES, INC.

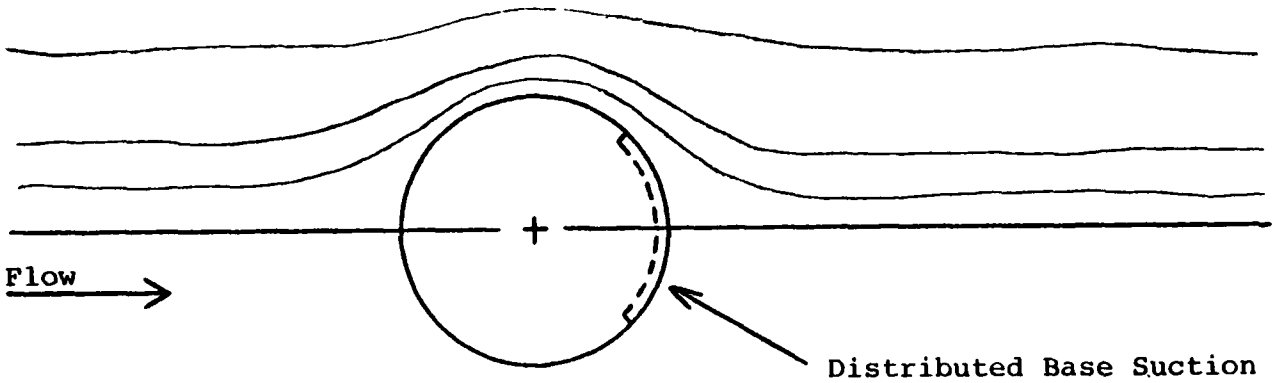

FIGURE III-4. BASE SUCTION. FROM deJONCKHEERE [3], PRESENTED BY SPECTRON DEVELOPMENT LABORATORIES, INC.

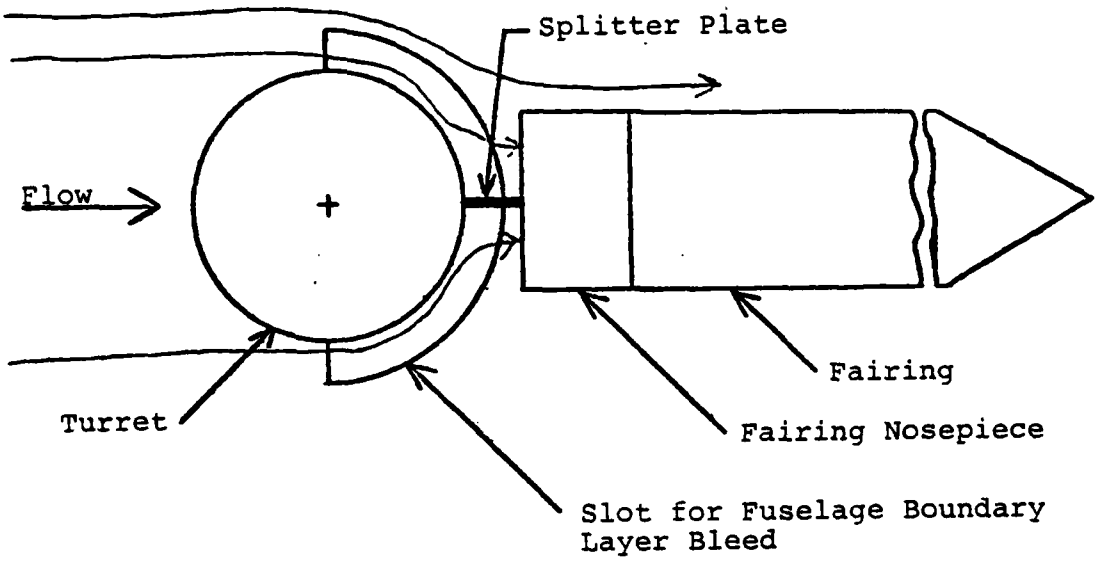

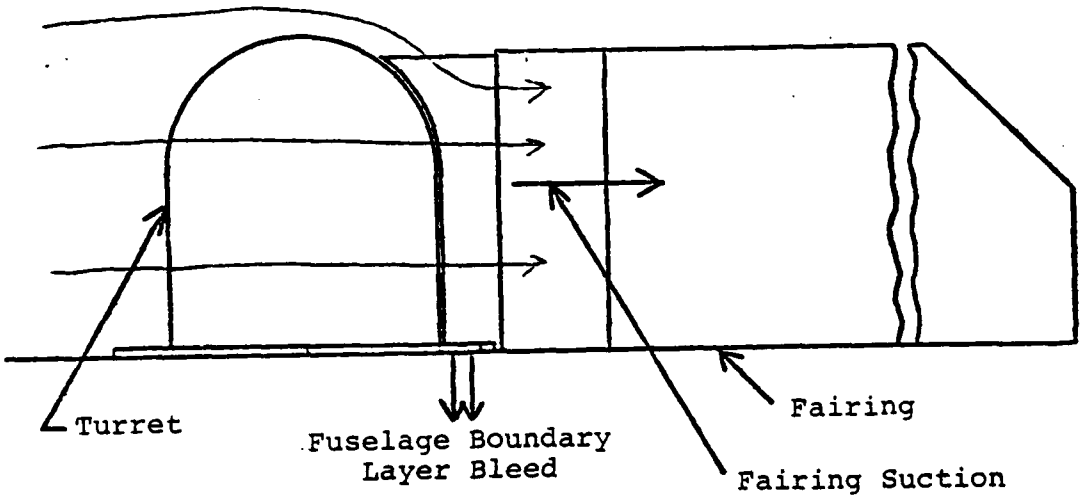

Base and Fairing Suction is caused by a blower mounted at the base of the fairing and connected via ducting.

FIGURE III-5. TURRET, FAIRING, AND FUSELAGE BOUNDARY LAYER BLEED.

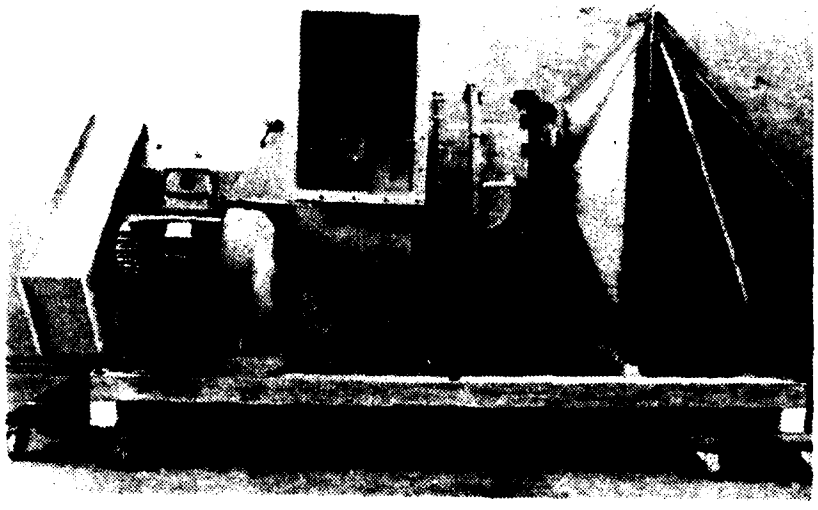

FIGURE IV-1. AEROVENT BLOWER AND SHEET-METAL DUCTING.

FIGURE IV-2. INLET CONTROL DAMPER ASSEMBLY.

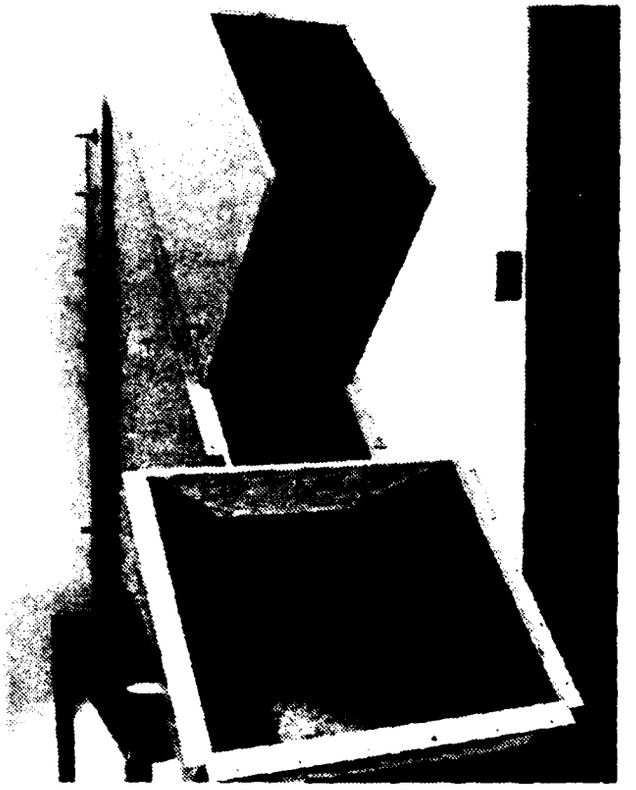

FIGURE IV-3. FAIRING DUCT ASSEMBLY AND PLENUM.

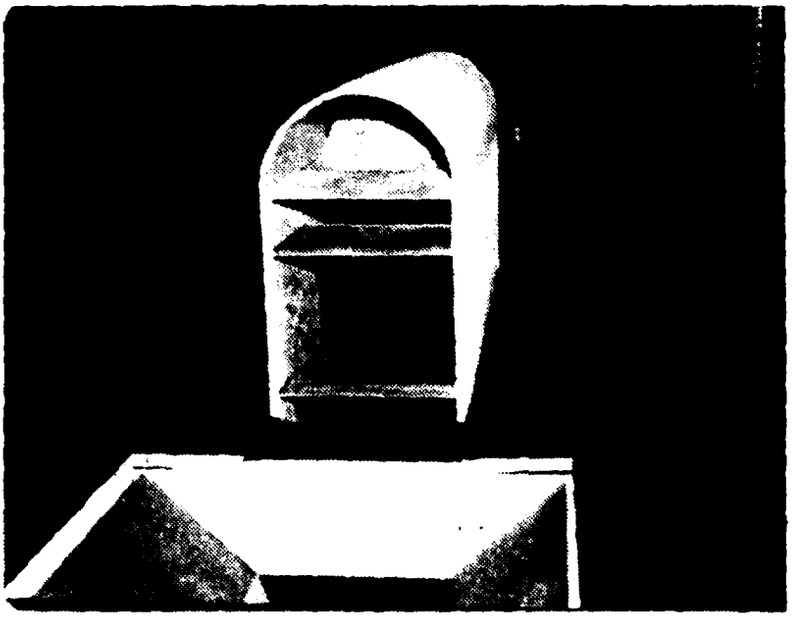

FIGURE IV-4. FAIRING DUCT ASSEMBLY AND PLENUM INSTALLED.

FIGURE IV-5. FAIRING NOSEPIECE.

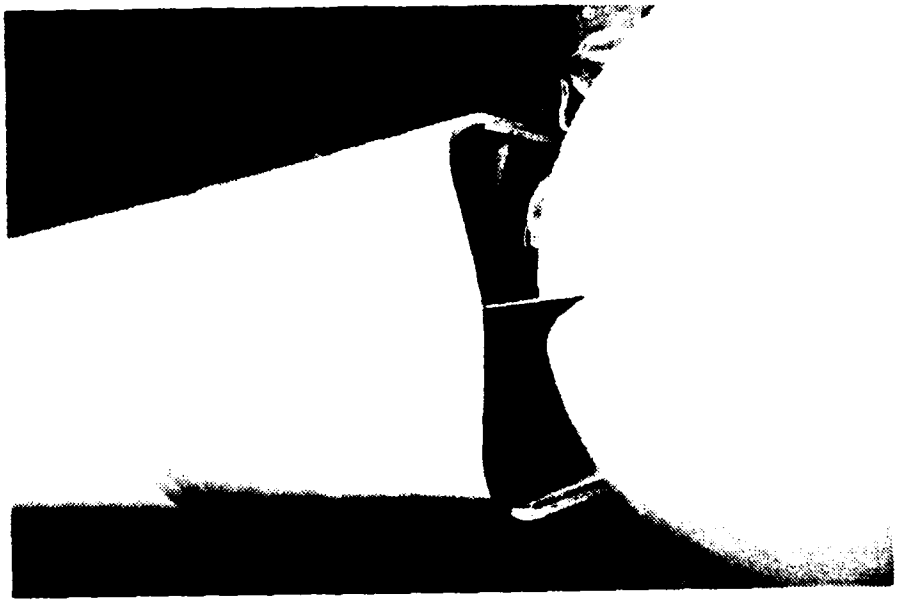

FIGURE IV-6. FAIRING NOSEPIECE-TURRET WITH 1.75-INCH SEPARATION.

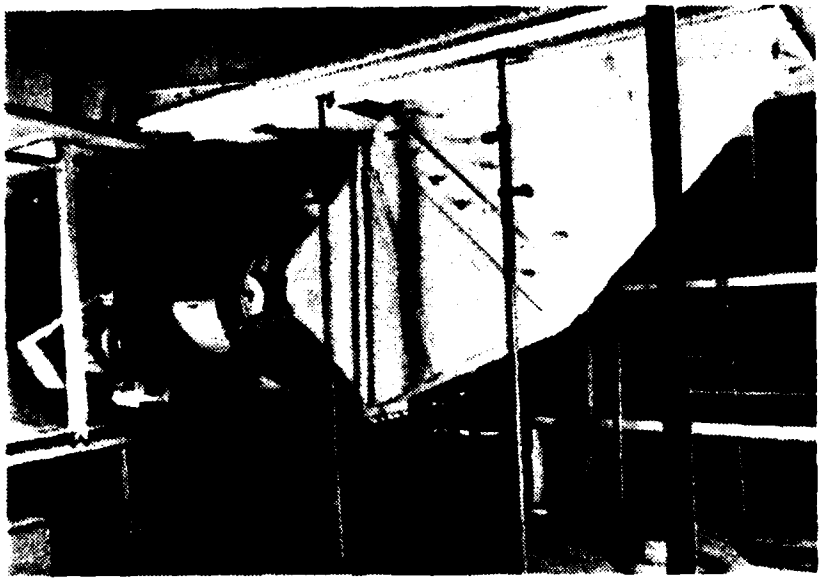

FIGURE IV-7. UNDER-TUNNEL ASSEMBLY, FRONT.

FIGURE IV-8. UNDER-TUNNEL ASSEMBLY, BACK.

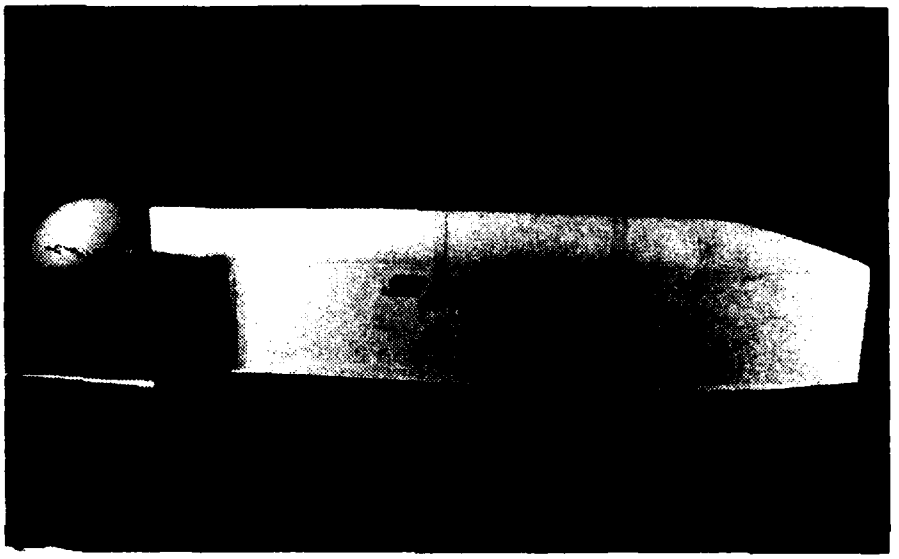

FIGURE IV-9. COMPLETE MODEL ASSEMBLY IN WINDTUNNEL, SIDEVIEW.

FIGURE IV-10. COMPLETE MODEL ASSEMBLY IN WINDTUNNEL, REARVIEW.

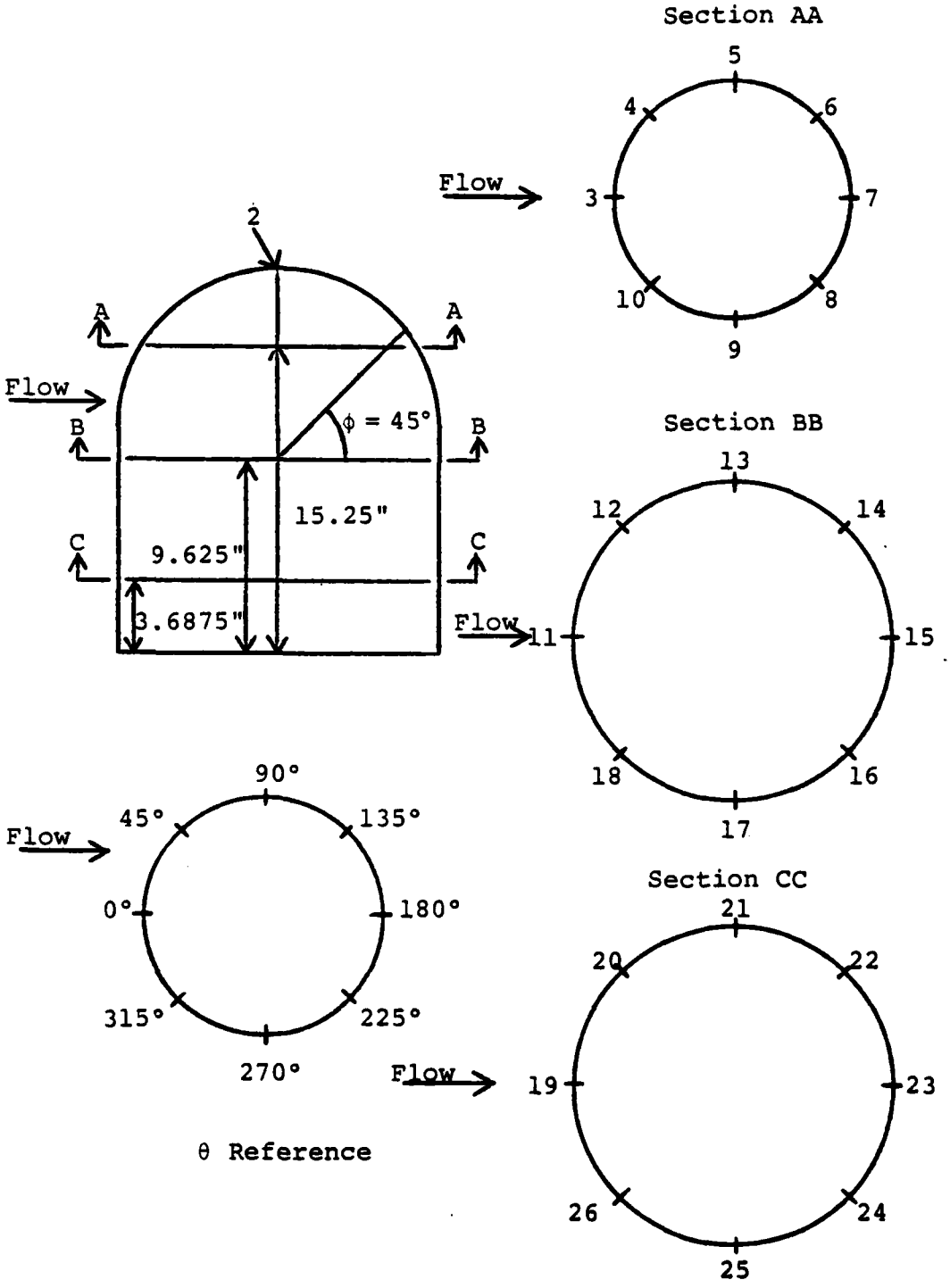

FIGURE V-1. TURRET PRESSURE TAP LOCATIONS.

FIGURE V-2. WIND TUNNEL DATA ACQUISITION SYSTEM.

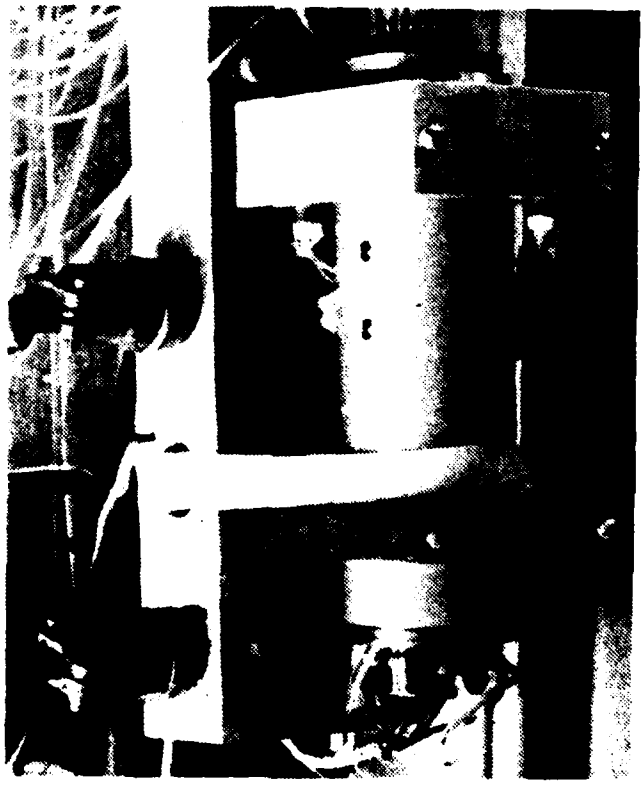

FIGURE V-3. SCANIVALVE.

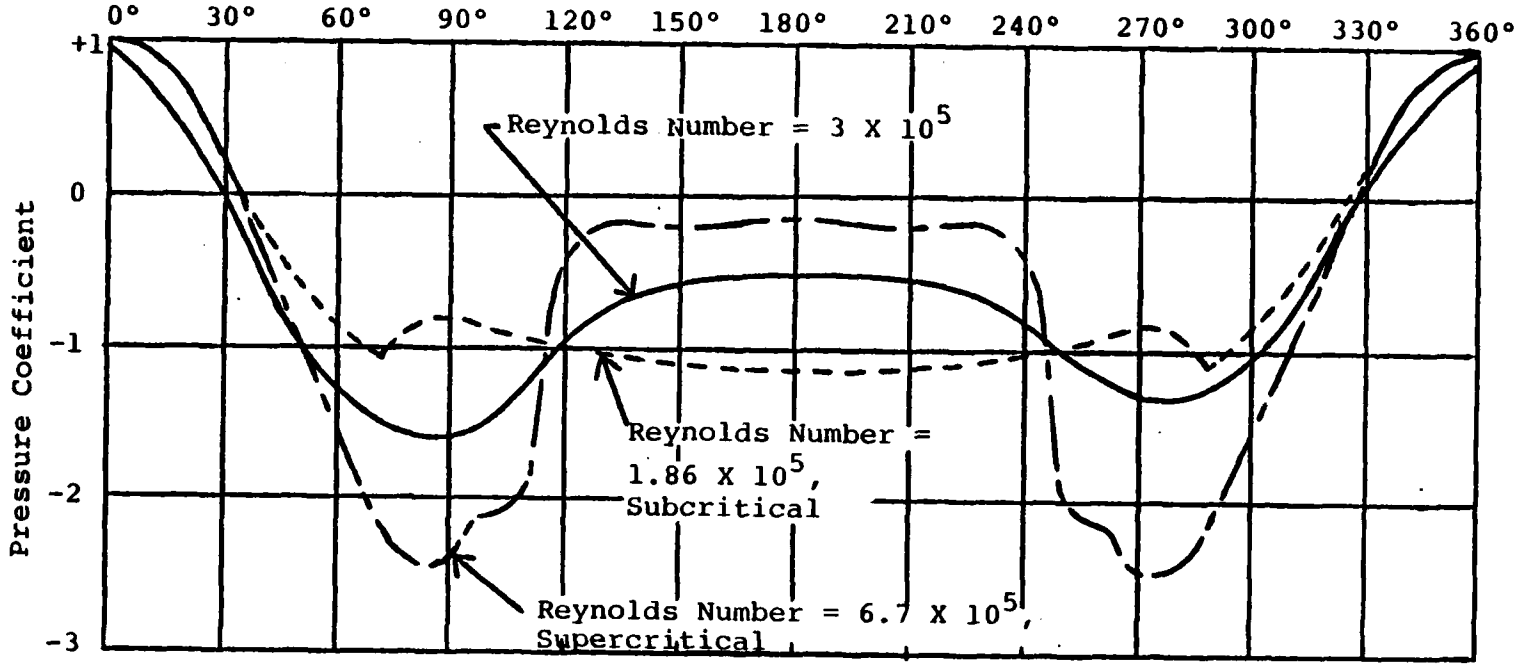

FIGURE VI-1. EXPERIMENTAL DATA PLOTTED WITH THE PRESSURE DISTRIBUTION ABOUT A CYLINDER IN SUBCRITICAL AND SUPERCTITICAL RANGE OF REYNOLDS NUMBER. FROM SCHLICTING [2].

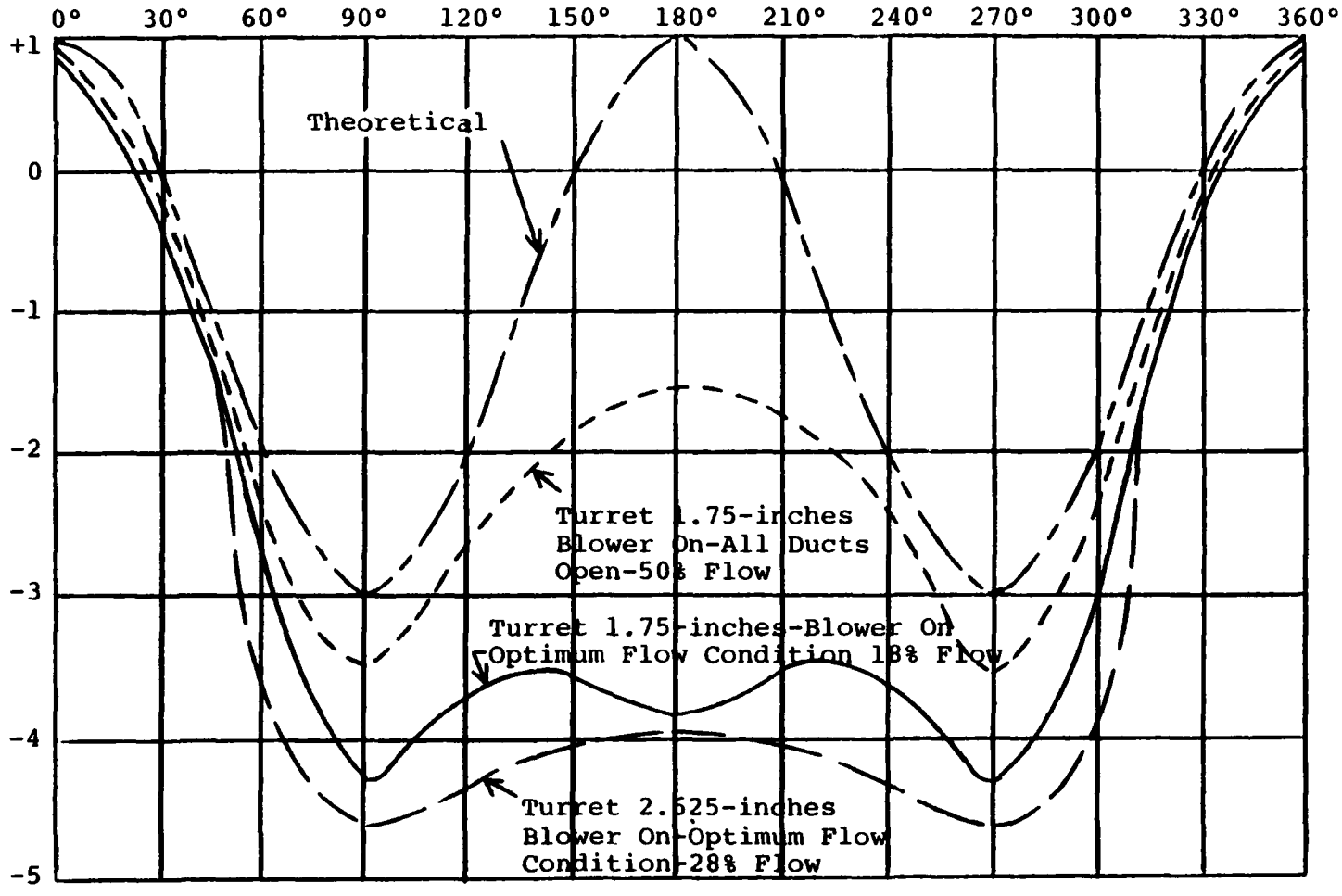

FIGURE VI-2. EXPERIMENTAL DATA PLOTTED WITH THEORETICAL PRESSURE DISTRIBUTION ABOUT A CYLINDER. FROM SCHLICTING [2].

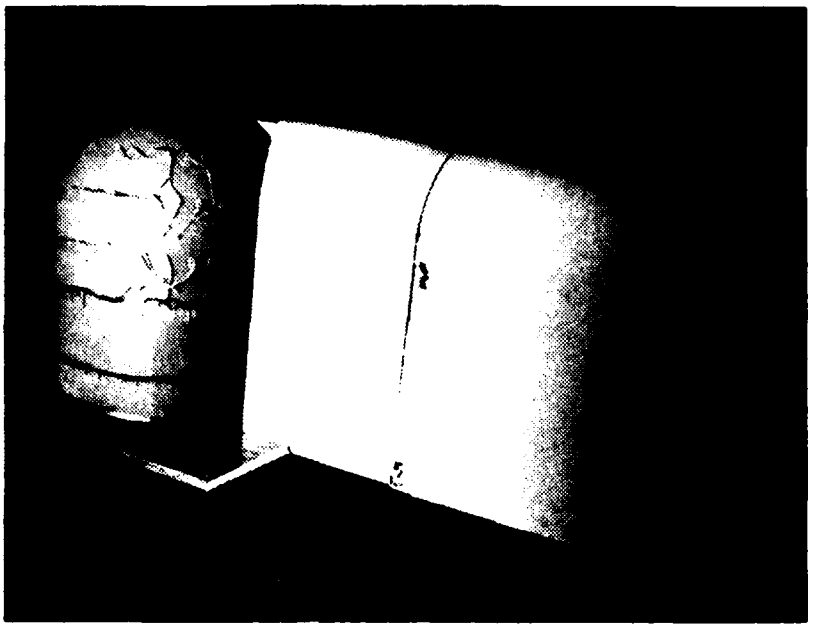

FIGURE VI-3. TURRET AND FAIRING-NOSEPIECE WITH WIND TUNNEL ON AND WITHOUT SUCTION.

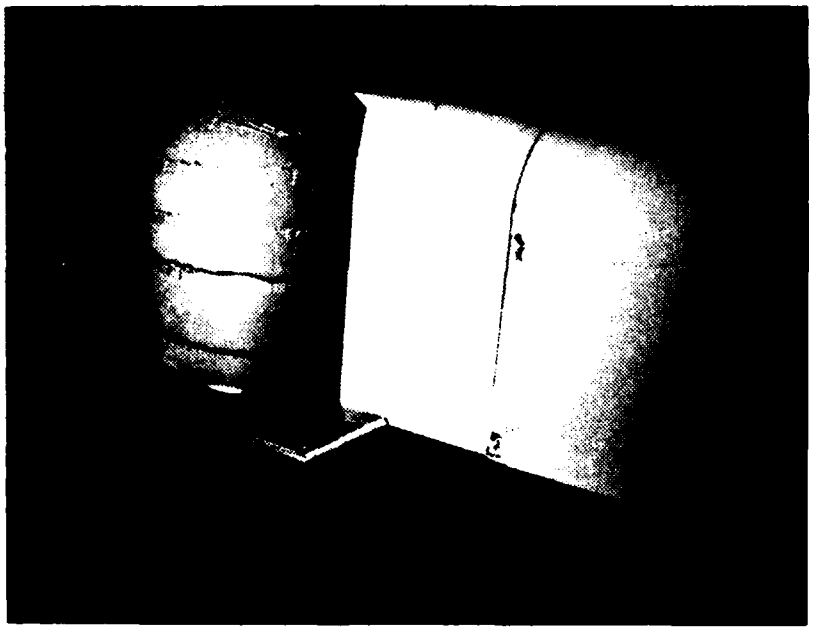

FIGURE VI-4. TURRET AND FAIRING-NOSEPIECE WITH WIND TUNNEL ON AND WITH SUCTION.

TABLE V-1

INSTRUMENTATION PRESSURE TAP
LOCATION LIST

PRESSURE TAP NUMBER	LOCATION
1	Ambient Pressure
2	Turret Hemisphere $\theta = 90°$
3	Turret Hemisphere $\theta = 0°$, $\phi = 45°$
4	Turret Hemisphere $\theta = 45°$, $\phi = 45°$
5	Turret Hemisphere $\theta = 90°$, $\phi = 45°$
6	Turret Hemisphere $\theta = 135°$, $\phi = 45°$
7	Turret Hemisphere $\theta = 180°$, $\phi = 45°$
8	Turret Hemisphere $\theta = 225°$, $\phi = 45°$
9	Turret Hemisphere $\theta = 270°$, $\phi = 45°$
10	Turret Hemisphere $\theta = 315°$, $\phi = 45°$
11	Turret Hemisphere $\theta = 0°$, $\phi = 0°$
12	Turret Hemisphere $\theta = 45°$, $\phi = 0°$
13	Turret Hemisphere $\theta = 90°$, $\phi = 0°$
14	Turret Hemisphere $\theta = 135°$, $\phi = 0°$

TABLE V-1 (Continued)

PRESSURE TAP NUMBER	LOCATION
15	Turret Hemisphere $\theta = 180°$, $\phi = 0°$
16	Turret Hemisphere $\theta = 225°$, $\phi = 0°$
17	Turret Hemisphere $\theta = 270°$, $\phi = 0°$
18	Turret Hemisphere $\theta = 315°$, $\phi = 0°$
19	Cylinder $\theta = 0°$
20	Cylinder $\theta = 45°$
21	Cylinder $\theta = 90°$
22	Cylinder $\theta = 135°$
23	Cylinder $\theta = 180°$
24	Cylinder $\theta = 225°$
25	Cylinder $\theta = 270°$
26	Cylinder $\theta = 315°$
27	Duct 1 (top) dynamic
28	Duct 1 (top) static
29	Duct 2 dynamic
30	Duct 2 static

TABLE V-1 (Continued)

PRESSURE TAP NUMBER	LOCATION
31	Duct 3 dynamic
32	Duct 3 static
33	Duct 4 dynamic
34	Duct 4 static
35	Duct 5 (bottom) dynamic Fuselage Boundary Layer Suction
36	Duct 5 (bottom) static Fuselage Boundary Layer Suction
37	Tunnel Wall 1 (front)
38	Tunnel Wall 2
39	Tunnel Wall 3
40	Tunnel Wall 4
41	Tunnel Wall 5
42	Tunnel Wall 6 (rear)
43	Impact Probe

TABLE VI-1

ESTIMATED REQUIRED FLOW RATE, Q_r, AND PRESSURE DIFFERENTIAL, ΔP_r, FOR FULL SCALE APPARATUS AT $M_\infty = 0.5$.

Separation Distance (inches)	Altitude (feet)	Ambient Pressure P(atm)	Ambient Speed of Sound, a (ft/sec)	ΔP_r (atm)	F	Q_r (cfm)
5.25	0	1.0	1116.43	0.2066	0.398	227,946
5.25	10,000	0.6878	1077.39	0.1421	0.398	220,087
5.25	20,000	0.4599	1036.94	0.0950	0.398	211,716
5.25	30,000	0.2978	994.85	0.0615	0.398	203,123
7.875	0	1.0	1116.43	0.2073	0.619	354,519
7.875	10,000	0.6878	1077.39	0.1426	0.619	342,297
7.875	20,000	0.4599	1036.94	0.0953	0.619	329,277
7.875	30,000	0.2978	994.85	0.0617	0.619	315,917

For a discussion of meaning of ΔP_r, F, and Q_r, refer to Appendix D.

LIST OF REFERENCES

1. Schonberger, James, Flow Control About an Airborne Laser Turret, M. S. Thesis, Naval Postgraduate School, Monterey, California, 1980.

2. Schlicting, Dr. Herman, Boundary-Layer Theory, p. 24, McGraw-Hill Book Co., 1968.

3. Schlicting, Dr. Herman, Boundary-Layer Theory, pp. 20-21, McGraw-Hill Book Co., 1968.

4. deJonckheere, Captain Richard, Control of Turbulent Separated Airflow about Aircraft Turrets, Workshop conducted at Air Force Weapons Laboratory, Kirtland Air Force Base, New Mexico, 10 and 11 March 1980.

5. Liepmann, H. W. and Roshko, A., Elements of Gas Dynamics, p. 407, John Wiley and Sons, Inc., 1957.

BIBLIOGRAPHY

Air Force Flight Dynamics Laboratory Report, AFFDL-TM-76-86, One-Fortieth Scale Wind Tunnel Test of the A.L.L. Cycle III/IV Fairing, Ronald E. Walterick, August 1976.

Air Force Flight Dynamics Laboratory Report, AFFDL-TM-78-46-FXM, High Incidence Angle Wind Tunnel Test of the A.L.L. Cycle III/IV Fairing, by Ronald E. Walterick, February 1978.

deJonckheere, Captain Richard, Control of Turbulent, Separated Airflow about Aircraft Turrets, Workshop presented at Air Force Weapons Laboratory, Kirtland Air Force Base, New Mexico, 10 and 11 March 1980.

Liepmann, H. W. and Roshko, A., Elements of Gas Dynamics, p. 407, John Wiley and Sons, Inc., 1957.

Schlicting, Dr. Herman, Boundary-Layer Theory, pp. 5-24, McGraw-Hill Book Co., 1968.

United States Air Force FACT SHEET, OIP No. 056.79 Current as of May 1979, The Department of Defense's (DOD) High Energy Laser (HEL) Program.

INITIAL DISTRIBUTION LIST

		No. Copies
1.	Defense Technical Information Center Cameron Station Alexandria, Virginia 22314	2
2.	Library, Code 0142 Naval Postgraduate School Monterey, California 93940	2
3.	Department Chairman, Code 67 Department of Aeronautics Naval Postgraduate School Monterey, California 93940	1
4.	Distinguished Professior Allen E. Fuhs Code 67Fu Department of Aeronautics Naval Postgraduate School Monterey, California 93940	10
5.	Lt. James Schonberger, USN 1920 Catherine Drive Bismark, North Dakota 58501	2
6.	Captain Richard deJonckheere, USAF AFWL, ARLB Kirtland Air Force Base New Mexico 87177	10
7.	Lt. Alan M. Mandigo, USN 208 Dunning Drive Camillus, New York 13031	2
8.	Dean W. M. Tolles Dean of Research Naval Postgraduate School Monterey, California 93940	1


DA1
FILM